Sulfur Tetrafluoride

Lewis Acid Behavior of SF_4: Synthesis, Characterization and Computational Study of SF_4 Adducts with Pyridine and Pyridine-Derivatives

Praveen Chaudhary,[a] James T. Goettel,[a] Hélène P.A. Mercier,[b] Shahin Sowlati-Hashjin,[a] Paul Hazendonk,[a] Michael Gerken[a,] *

Contribution from the Canadian Centre for Research in Advanced Fluorine Technologies, University of Lethbridge, Lethbridge, Alberta T1K 3M4, Canada; Department of Chemistry and Biochemistry, The University of Lethbridge, Lethbridge, Alberta T1K 3M4, Canada; and Department of Chemistry, McMaster University, Hamilton, Ontario L8S 4M1.

* Corresponding author. Tel.: +1-403-329-2173; fax: +1-403-329-2057. *e-mail address*: michael.gerken@uleth.ca.

[a] University of Lethbridge

[b] McMaster University

Table of Content

Fluorine Chemistry

Lewis Acid Behavior of SF_4: Synthesis, Characterization and Computational Study of SF_4 Adducts with Pyridine and Pyridine-Derivatives

Praveen Chaudhary, James T. Goettel, Dr. Hélène P.A. Mercier, Shahin Sowlati-Hashjin, Prof. Paul Hazendonk, Prof. Michael Gerken

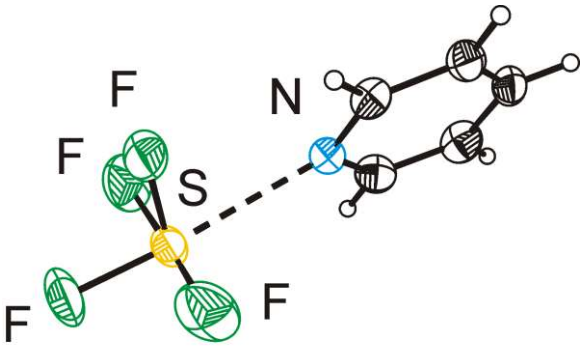

$SF_4 \cdot NC_5H_5$

Sulfur Tetrafluoride is weakly Lewis acidic toward organic nitrogen-bases. Adducts with pyridine, 4-methylpyridine, 2,6-dimethylpyridine, and 4-dimethylaminopyridine are only stable at low temperature and are studied by Raman and NMR spectroscopy and DFT calculations. Crystal structures of $SF_4 \cdot NC_5H_5$, $SF_4 \cdot 4\text{-}NC_5H_4(CH_3)$, and $SF_4 \cdot 4\text{-}NC_5H_4N(CH_3)_2$ adducts conclusively show S---N interactions between SF_4 and the organic bases.

Abstract

Sulfur tetrafluoride was shown to act as a Lewis acid towards organic nitrogen-bases, such as pyridine, 2,6-dimethylpyridine, 4-methylpyridine, and 4-dimethylaminopyridine. The $SF_4 \cdot NC_5H_5$, $SF_4 \cdot 2,6\text{-}NC_5H_3(CH_3)_2$, $SF_4 \cdot 4\text{-}NC_5H_4(CH_3)$, and $SF_4 \cdot 4\text{-}NC_5H_4N(CH_3)_2$ adducts can be isolated as solids that are stable below –45 °C. The Lewis acid-base adducts were characterized by low-temperature Raman spectroscopy and the vibrational bands were fully assigned with the aid of density-functional-theory (DFT) calculations. The electronic structures obtained from the DFT calculations were analyzed by the quantum theory of atoms in molecules (QTAIM). The crystal structures of $SF_4 \cdot NC_5H_5$, $SF_4 \cdot 4\text{-}NC_5H_4(CH_3)$, and $SF_4 \cdot 4\text{-}NC_5H_4N(CH_3)_2$ revealed weak S---N dative bonds with nitrogen coordinating in the equatorial position of SF_4. Based on the QTAIM analysis, the non-bonded valence shell charge concentration on sulfur, which represents the lone pair, is only slightly distorted by the weak dative S---N bond. No evidence for adducts between quinoline or isoquinoline with SF_4 was found by low-temperature Raman spectroscopy.

Keywords: Sulfur, Fluorine, structure elucidation, Lewis acids/bases, Raman spectroscopy

Introduction

Recently we reported the synthesis of the Lewis acid-base adduct between SF_4 and $N(C_2H_5)_3$ and its unambiguous characterization by low-temperature Raman spectroscopy and X-ray crystallography.[1] Previous evidence for the Lewis acidity of SF_4 towards nitrogen-bases was mainly based on vapor pressure measurements, suggesting the existence of 1:1 adducts between SF_4 and NC_5H_5 and $N(C_2H_5)_3$.[2] An elemental analysis study detected the $SF_4 \cdot NC_5H_5$ adduct and claimed the existence of distinct $SF_4 \cdot 2NC_5H_5$, $SF_4 \cdot 4NC_5H_5$, and $SF_4 \cdot 8NC_5H_5$ adducts at −78 °C, but no further experimental evidence has been provided for these latter adducts.[3] A matrix-isolation infrared study revealed only one to three vibrational bands attributed to each of the adducts, $SF_4 \cdot NC_5H_5$, $SF_4 \cdot NH_3$, $SF_4 \cdot CH_3NH_2$, and $SF_4 \cdot OC(CH_3)_2$.[4] Extensive overlap of the infrared bands of product and reactant precluded definitive identification. In contrast, conclusive evidence for the Lewis-acid behavior of SF_4 towards fluoride ions has been established by the synthesis of $[N(CH_3)_4][SF_5]$,[5] $Cs[SF_5]$,[6] $Rb[SF_5]$,[7] $[((CH_3)_2N)_3S][SF_5]$,[8] and $[Cs(18\text{-crown-}6)_2][SF_5]$.[9] The crystal structures of $Rb[SF_5]$,[7] $Cs_6[SF_5]_4[HF_2]_2$,[7] $[Cs(18\text{-crown-}6)_2][SF_5]$,[9] and $[HNC_5H_3(CH_3)_2]_2F\cdots SF_4[SF_5] \cdot 3SF_4$[10] have confirmed the expected square pyramidal geometry of the $[SF_5]^-$ anion.

Sulfur tetrafluoride is an important covalent binary main-group fluoride which has seen routine use in inorganic and organic chemistry.[11] Since SF_4 has been used as a deoxofluorinating agent in organic chemistry, the study of its interactions with organic Lewis bases and their subsequent impact on its structure is essential to gain deep insights into the mechanism of deoxofluorination.

The goal of the present study was to investigate the Lewis acid behavior of SF_4 towards a variety of organic nitrogen bases without α-hydrogens. Ammonia, primary and secondary amines

undergo condensation reactions with SF_4 releasing HF and forming covalent S–N bonds. For example, SF_4 reacts with CH_3NH_2 at low temperature, yielding $CH_3N{=}SF_2$.[12] Hence, pyridine and its derivatives were chosen as appropriate Lewis bases, alongside the previously studied tertiary amine, $N(C_2H_5)_3$.

Results and Discussion

Synthesis and Properties of SF_4 Adducts

Pyridine, 2,6-dimethylpyridine, and 4-methylpyridine were allowed to react with excess SF_4 at –80 °C yielding colorless, clear solutions. Removal of excess SF_4 under dynamic vacuum at –80 °C gave rise to white solids, which were shown to be Lewis acid-base adducts by low-temperature Raman spectroscopy (eq. 1). The reaction of excess SF_4 with 4-dimethylaminopyridine (DMAP) at –80 °C yielded a white suspension, from which $SF_4{\cdot}4\text{-}NC_5H_4N(CH_3)_2$, in admixture with unreacted base, was isolated upon removal of volatiles at –80 °C. The incomplete reaction of DMAP with SF_4 was attributed to the insolubility of the adduct in liquid SF_4. The solid adducts were stable under dynamic vacuum below –45 °C and were studied by low-temperature Raman spectroscopy. When the adducts were warmed to –35 °C under dynamic vacuum, SF_4 was removed and the nitrogen-bases were recovered.

$$SF_4 + B \underset{-35\ ^\circ C}{\overset{-80\ ^\circ C}{\rightleftharpoons}} SF_4{\cdot}B \qquad (1)$$

$$B = NC_5H_5,\ 2,6\text{-}NC_5H_3(CH_3)_2,\ 4\text{-}NC_5H_4(CH_3),\ 4\text{-}NC_5H_4N(CH_3)_2$$

In the case of 2,6-dimethylpyridine and 4-methylpyridine, traces of $[HF_2]^-$ were observed by Raman spectroscopy after removal of SF_4, likely resulting from traces of water in the reaction

mixture. The mass balances of these reactions support the formation of 1:1 adducts. The adducts of pyridine, 2,6-dimethylpyridine, 4-methylpyridine, and DMAP are soluble in CH_2Cl_2 and toluene at –60 °C. The reactions of SF_4 with quinoline and isoquinoline were also studied at low-temperature; however, under the current conditions, no Raman spectroscopic evidence for the formation of Lewis acid-base adducts was found, where bands attributed to the reactants persisted at –100 °C. The donor strengths of quinoline and isoquinoline are most likely insufficient to favor formation of stable adducts with the weak Lewis acid SF_4.

Raman Spectroscopy

The Raman spectra of solid $SF_4{\cdot}NC_5H_5$, $SF_4{\cdot}4\text{-}NC_5H_4(CH_3)$, $SF_4{\cdot}2,6\text{-}NC_5H_3(CH_3)_2$, and $SF_4{\cdot}4\text{-}NC_5H_4N(CH_3)_2$ (Figure 1) were recorded at –100 °C. The observed and calculated vibrational frequencies of the N---SF_4 moiety in the four adducts are listed in Table 1, together with their assignments. Complete lists of observed and calculated vibrational frequencies for all the adducts are given in the Supporting Information along with their assignments (Tables S1 to S4). The assignments for the Raman bands of the adducts are based on density-functional-theory (DFT) calculations, which predicted frequencies that were overall in good agreement with those observed. The assignments were supported by comparison with the assignment of the bands of the free Lewis bases and those of neat SF_4.

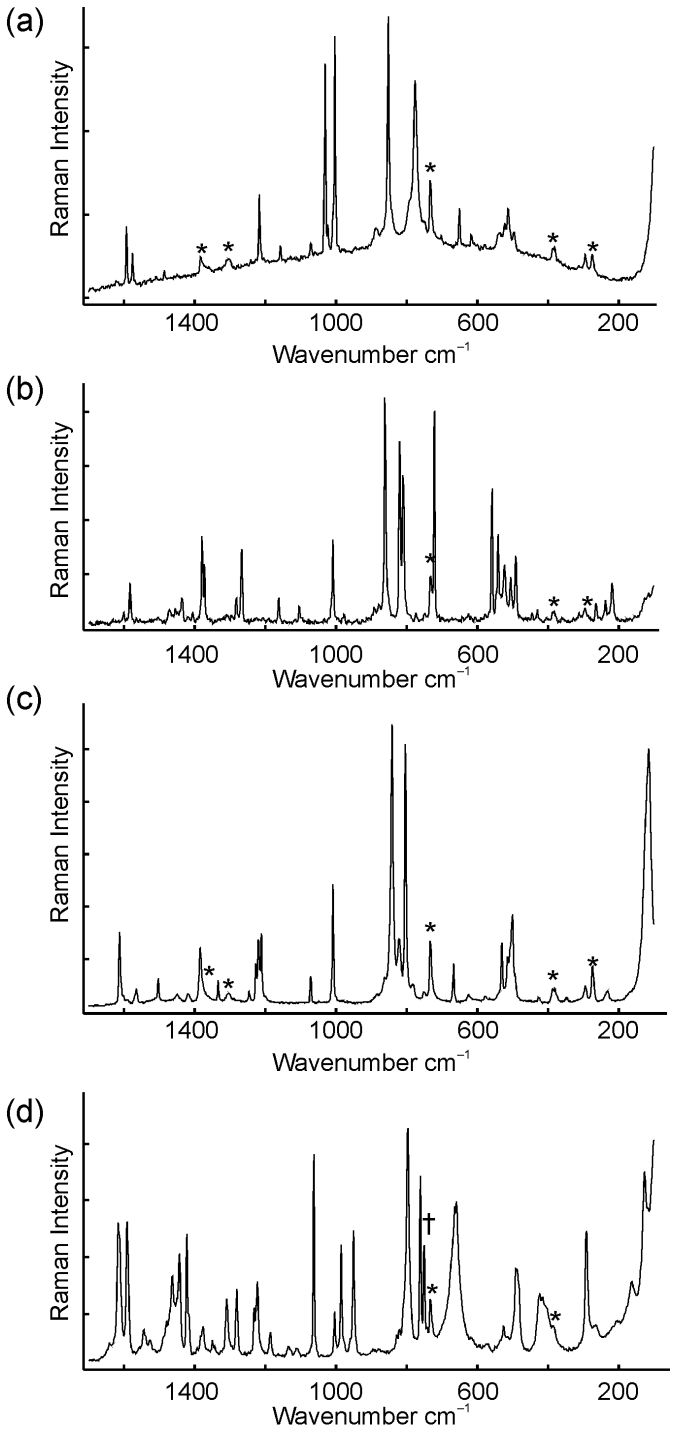

Figure 1. Raman spectra of (a) $SF_4 \cdot NC_5H_5$, (b) $SF_4 \cdot 2,6\text{-}NC_5H_3(CH_3)_2$, (c) $SF_4 \cdot 4\text{-}NC_5H_4(CH_3)$, and (d) $SF_4 \cdot 4\text{-}NC_5H_4N(CH_3)_2$ at −100 °C. Asterisks (*) and dagger (†) denote bands arising from the FEP sample tube and DMAP, respectively.

Table 1. Observed and Calculated Frequencies and Their Assignments for the N---SF_4 Moieties in the SF_4·2,6-$NC_5H_3(CH_3)_2$, SF_4·NC_5H_5, SF_4·4-$NC_5H_4(CH_3)$, and SF_4·4-$NC_5H_4N(CH_3)_2$ Adducts

SF_4·2,6-$NC_5H_3(CH_3)_2$		SF_4·NC_5H_5		SF_4·4-$NC_5H_4(CH_3)$		SF_4·4-$NC_5H_4N(CH_3)_2$		assignments[c]
exptl[a]	calcd[b]	exptl[a]	calcd[b]	exptl[a]	calcd[b]	exptl[a]	calcd[b]	
861(100)	838(82)[119]	852(100) 842sh	833(67)[151]	841(100)	822(59)[165]	797(100)	813(84)[158]	$\nu(S–F_1)$
820(81) 810(65)	793(75)[316]	776(71)	779(68)[380]	804(93)	758(97)[443]	659(67)	732(136)[550]	$\nu(S–F_2)$
n.o.	666(1)[512]	702(3)	681(1)[348]	625(3)	644(2)[466]	n.o	634(2)[444]	$\nu(S–F_3) - \nu(S–F_4)$[d]
523(25)	516(9)[1]	522(12) 513(19)	518(6)[<1]	501(31)	503(5)[10]	491(36)	500(7)[<1]	$\nu(S–F_3) + \nu(S–F_4)$
505(20)	490(<1)[10]	497(9)	485(1)[39]	494sh	480(2)[41]	487(35)	477(3)[42]	$\delta(F_1S_1F_2) + \delta(F_3S_1F_4)$
491(29)	488(2)[28]	n.o.	481(<1)[7]	n.o.	475(<1)[13]	n.o.	470(<1)[17]	$\delta(F_1S_1F_3) - \delta(F_1S_1F_4) + \rho_w(F_1S_1F_2)$
n.o.	422(<1)[<0.1]	n.o.	394(<1)[<1]	n.o.	386(<1)[2]	n.o.	371(<1)[3]	$\rho_t(F_1S_1F_2) + \delta(F_2S_1F_3) - \delta(F_2S_1F_4)$[d]
n.o.	331(<1)[15]	n.o.	342(<1)[16]	n.o.	345(<1)[16]	n.o.	356(<1)[15]	$\rho_r(F_1S_1F_2) + \rho_w(F_3S_1F_4)$[e]
237(9)	233(3)[<1]	274(9)	252(2)[1]	274(12)	254(3)[1]	291(49)	257(5)[<1]	$\delta(F_1S_1F_2) + \rho_w(F_3S_1F_4)$
n.o.	56(1)[2]	n.o.	70(1)[<0.1]	n.o.	68(1)[9]	n.o.	70(<1)[13]	$\nu(S–N)$

[a] Obtained by Raman spectroscopy from solid samples in FEP tubing at −100 °C. The abbreviations denote not observed (n.o.) and shoulder (sh). Complete lists of Raman frequencies are given in the Supporting Information (Tables S1 to S4). Values in parentheses denote relative intensities. [b] Calculated at the B3LYP/aug-cc-pVTZ level of theory. Unscaled Raman intensities, in $Å^4\ u^{-1}$, are given in parentheses; infrared intensities, in km mol^{-1}, are given in square brackets. [c] The abbreviations denote symmetric (s), antisymmetric (as), stretch (ν), bend (δ), twist (ρ_t), wagging (ρ_w), and rock (ρ_{rock}). The numbering scheme refers to that used in Figure 2. [d] In the SF_4·NC_5H_5 adduct, the SF_4 mode is coupled with deformation modes of the pyridine moiety. [e] In the SF_4·4-$NC_5H_4N(CH_3)_2$, this mode is coupled with the $\rho_r(CH_3)$ vibration.

The Raman spectra of the solid adducts of SF_4 with NC_5H_5, 4-$NC_5H_4CH_3$, 2,6-$NC_5H_3(CH_3)_2$, and 4-$NC_5H_4N(CH_3)_2$ show distinct Raman bands differing from those of SF_4 and the free *N*-bases, which are attributed to the *N*-base and SF_4 moieties of the SF_4·base adducts. The DFT calculations show that vibrational coupling between modes involving the SF_4 moiety and the *N*-base occurs on a few occasions. A number of bands attributed to the *N*-base moieties in the adducts are significantly shifted with respect to those of the free bases. These shifts are consistent with the formation of Lewis acid-base adducts. The most indicative feature for adduct formation is the high-frequency shift of the very strong Raman band attributable to the NC_5 ring breathing mode. The frequency of the NC_5 ring breathing mode in pyridine has been used to assess the strength of the Lewis acid-base interaction for adducts of pyridine.[13,14] While this mode is assigned to the Raman band at 990 cm^{-1} in free pyridine, the corresponding band for SF_4·NC_5H_5 appears at 1003 cm^{-1}. The frequency shift in this mode upon adduct formation (13 cm^{-1}) is in excellent agreement with the predicted shift (14 cm^{-1}). The band associated with the ring breathing mode in the SF_4·NC_5H_5 adduct, however, occurs at a significantly reduced frequency over those in the pyridine adducts of stronger Lewis acids, such as WSF_4·NC_5H_5 (1016 cm^{-1})[14] and BF_3·NC_5H_5 (1026 cm^{-1}),[15] reflecting the relative weakness of the Lewis acid-base interaction between SF_4 and pyridine. This weakness is further corroborated by the low dissociation temperature of the adduct (vide supra). The ring breathing modes of the SF_4 adducts of 4-$NC_5H_4(CH_3)$ (1009 cm^{-1}), 2,6-$NC_5H_3(CH_3)_2$, (1009 cm^{-1}) and 4-$NC_5H_4N(CH_3)_2$ (1004 cm^{-1}) show similar shifts with respect to the free bases, *i.e.*, 11, 11, and 19 cm^{-1}, respectively.

Upon reaction with a nitrogen-base, the broad Raman bands of neat liquid SF_4 at –100 °C disappear and a set of relatively sharp bands are observed in the S–F stretching region of the Raman spectra at –100 °C. This can be explained by the formation of adducts that are solid at this

temperature. Numerous reports have been published about the vibrational spectra of SF_4 in the gas, liquid, and solid phases, as well as in N_2, Ar, and Ne matrices.[16] The assignment of the normal modes to the vibrational frequencies has been subject to several revisions, resulting in the final mode descriptions of the complete set of vibrational frequencies of gaseous SF_4 published by Christe *et al.*[17] The latter vibrational assignments were based on calculations of vibrational frequencies at the same level of theory used for the SF_4 adducts performed in the current study. The complete set of gaseous frequencies will be used for comparison in the following discussion. Any changes in vibrational frequencies caused by changes in the phase of SF_4 are smaller than those discussed in the present paper when comparing the adducts with free SF_4. When compared to the Raman bands of free SF_4, the S–F stretching bands of the adducts are shifted to significantly lower frequencies. These shifts are in agreement with the donation of electron density from a Lewis base to sulfur, making the S–F bonds more ionic in nature. Two isomers are conceivable for the $SF_4 \cdot N$-base adducts (Scheme I), both exhibiting a square-pyramidal geometry about sulfur: Isomer A with the base coordinating in the equatorial position of the seesaw-geometric SF_4 moiety and isomer B with the base in the axial position and a nearly planar SF_4 moiety.

Isomer A Isomer B

Scheme I, B = base

The excellent agreement between the calculated vibrational frequencies for isomer A with their experimental values supports the formation of isomer A. The general retention of the local

seesaw geometry of free SF_4 in isomer A is in agreement with the observation that the Raman bands of the SF_4 moiety are shifted with respect to free SF_4, while leaving their relative intensities comparatively unchanged. The different symmetry of the SF_4 moiety in isomer B should lead to significant changes in the intensity pattern of bands in the SF stretching region. As a matter of fact, isomer A was observed by X-ray crystallography for the $SF_4 \cdot NC_5H_5$, $SF_4 \cdot 4\text{-}NC_5H_4(CH_3)$, and $SF_4 \cdot 4\text{-}NC_5H_4N(CH_3)_2$ adducts and was found to be the global energy minimum in geometry optimizations (vide infra). In contrast, isomer B was predicted to be a local energy minimum by DFT calculations for $SF_4 \cdot NC_5H_5$ and $SF_4 \cdot 4\text{-}NC_5H_4(CH_3)$ (vide infra) (Tables S5 and S6), thus this isomer can be ruled out on the basis of the predicted vibrational frequencies and observed Raman intensities of the SF_4 stretching bands. The absence of a second set of Raman bands attributable to the other isomer precludes the need to consider two co-existing isomers; therefore, the Raman spectra will be discussed in terms of a single isomer of type A.

Upon adduct formation, the equatorial fluorine atoms in free SF_4 become the non-symmetry-related F_1 and F_2, whereas the axial fluorines become F_3 and F_4. The symmetric (892 cm^{-1}) and antisymmetric (867 cm^{-1}) stretching frequencies for the equatorial SF_2 group in free SF_4 are shifted to lower frequencies between 861 and 797 cm^{-1} for $\nu(S–F_1)$ and between 810 and 659 cm^{-1} for $\nu(S–F_2)$ in the adducts, respectively. The shift to lower frequencies was accurately predicted by the DFT calculations (SF_4: 856 and 825 cm^{-1}; adducts: 838, 833, 822, 813 cm^{-1} ($\nu(S–F_1)$) and 793, 779, 758, and 732 cm^{-1} ($\nu(S–F_2)$). The degree of coupling between $\nu(S–F_1)$ and $\nu(S–F_2)$ was predicted to be negligible. The splitting of the $\nu(S–F_2)$ mode into two bands (810 and 820 cm^{-1}) in the Raman spectrum of $SF_4 \cdot 2,6\text{-}NC_5H_3(CH_3)_2$ is tentatively attributed to vibrational coupling within the crystallographic unit cell. The symmetric stretching band for the axial SF_2 group is also shifted to lower frequencies from 558 cm^{-1} in neat SF_4 to frequencies ranging from

523 to 491 cm^{-1} ($\nu(S–F_3) + \nu(S–F_4)$) in the adducts (calcd: 535 cm^{-1} (SF_4); 516, 518, 503, 500 cm^{-1} (adducts)). The corresponding antisymmetric mode, $\nu(S–F_3) - \nu(S–F_4)$, expected to be weak in the Raman spectrum, occurs at higher frequency than the symmetric mode, and was observed as weak bands for $SF_4 \cdot NC_5H_5$ (702 cm^{-1}) and $SF_4 \cdot 4\text{-}NC_5H_4(CH_3)$ (625 cm^{-1}). The observed shift to lower frequency from free SF_4 to the adducts (SF_4: 730 cm^{-1}; adducts: 702, 625 cm^{-1}) was reproduced computationally (SF_4: 703 cm^{-1}; adducts: 666, 681, 644, 634 cm^{-1}).

Crystal Structures of $SF_4 \cdot NC_5H_5$, $SF_4 \cdot NC_5H_4CH_3$ and $SF_4 \cdot NC_5H_4N(CH_3)_2$

The $SF_4 \cdot NC_5H_5$ and $SF_4 \cdot 4\text{-}NC_5H_4(CH_3)$ adducts were crystallized from SF_4 solvent at –80 °C. Because of the insolubility of $SF_4 \cdot 4\text{-}NC_5H_4N(CH_3)_2$ in SF_4, crystals of this adduct were grown from CH_2Cl_2. Attempts to grow crystals of the 2,6-dimethylpyridine adduct suitable for X-ray crystallography were unsuccessful. Selected crystallographic data for $SF_4 \cdot NC_5H_5$, $SF_4 \cdot 4\text{-}NC_5H_4(CH_3)$, and $SF_4 \cdot 4\text{-}NC_5H_4N(CH_3)_2$ are given in Table 2; notable bond lengths and angles are listed in Table 3.

Table 2. Crystallographic Data for $SF_4 \cdot NC_5H_5$, $SF_4 \cdot 4\text{-}NC_5H_4(CH_3)$, and $SF_4 \cdot 4\text{-}NC_5H_4N(CH_3)_2$

chem formula	$SF_4 \cdot NC_5H_5$	$SF_4 \cdot 4\text{-}NC_5H_4(CH_3)$	$SF_4 \cdot 4\text{-}NC_5H_4N(CH_3)_2$
space group	$P2_1/n$	$Pbcn$	$P2_1/c$
a (Å)	10.505(2)	20.532(15)	8.156(4)
b (Å)	5.6081(13)	11.017(8)	8.421(4)
c (Å)	12.655(3)	7.432(5)	13.935(7)
β (°)	98.017(3)	90	90.279(5)
molecules/unit cell	4	8	2
mol wt (g mol^{-1})	187.16	201.19	230.23
calcd density (g cm^{-3})	1.684	1.590	1.602
T (°C)	−130	−120	−120
μ (mm^{-1})	0.443	0.395	0.362
R_1[a]	0.0404	0.0457	0.0515
wR_2[b]	0.0827	0.1086	0.1340

[a] R_1 is defined as $\Sigma||F_o| - |F_c||/\Sigma|F_o|$ for $I > 2\sigma(I)$. [b] wR_2 is defined as $[\Sigma[w(F_o^2 - F_c^2)^2]/\Sigma w(F_o^2)^2]^{1/2}$ for $I > 2\sigma(I)$.

Table 3. Selected Experimental and Calculated Metric Parameters for $SF_4 \cdot NC_5H_5$, $SF_4 \cdot 4\text{-}NC_5H_4(CH_3)$, $SF_4 \cdot 2,6\text{-}NC_5H_4(CH_3)$, and $SF_4 \cdot 4\text{-}NC_5H_4N(CH_3)_2$

$SF_4 \cdot NC_5H_5$					
Bond lengths, Å			Angles, deg		
	exptl	calcd[a]		exptl	calcd[a]
S–F_1	1.5345(15)	1.580	F_1–S–F_2	95.57(8)	95.5
S–F_2	1.5599(14)	1.599	F_1–S–F_3	86.47(10)	86.9
S–F_3	1.677(2)	1.712	F_1–S–F_4	87.08(10)	86.9
S–F_4	1.652(2)	1.712	F_3–S–F_4	172.60(10)	173.5
S---N	2.514(2)	2.573	N–S–F_1	78.34(7)	79.9
			N–S–F_2	173.72(8)	175.4
$SF_4 \cdot 4\text{-}NC_5H_4(CH_3)$					
Bond lengths, Å			Angles, deg		
	exptl	calcd[a]		exptl	calcd[a]
S–F_1	1.526(2)	1.581	F_1–S–F_2	95.74(9)	95.1
S–F_2	1.551(2)	1.601	F_1–S–F_3	87.07(13)	86.9
S–F_3	1.660(2)	1.714	F_1–S–F_4	86.22(9)	86.9
S–F_4	1.665(2)	1.714	F_3–S–F_4	172.36(11)	173.4
S---N	2.513(3)	2.546	N–S–F_1	79.00(8)	80.0
			N–S–F_2	174.61(9)	175.2
$SF_4 \cdot 2,6\text{-}NC_5H_3(CH_3)_2$					
Bond lengths, Å			Angles, deg		
	exptl	calcd[a]		exptl	calcd[a]
S–F_1	-	1.575	F_1–S–F_2	-	98.6
S–F_2	-	1.588	F_1–S–F_3	-	87.5
S–F_3	-	1.697	F_1–S–F_4	-	87.2
S–F_4	-	1.700	F_3–S–F_4	-	172.3
S---N	-	2.954	N–S–F_1	-	81.4
			N–S–F_2	-	177.9
$SF_4 \cdot 4\text{-}NC_5H_4N(CH_3)_2$					
Bond lengths, Å			Angles, deg		
	exptl	calcd[a]		exptl	calcd[a]
S–F_1	1.561(2)	1.585	F_1–S–F_2	89.98(11)	93.8
S–F_2	1.616(2)	1.611	F_1–S–F_3	85.26(15)	86.7
S–F_3	1.682(2)	1.720	F_1–S–F_4	84.62(12)	86.7
S–F_4	1.684(2)	1.720	F_3–S–F_4	169.70(14)	173.3
S---N	2.141(2)	2.453	N–S–F_1	82.55(10)	80.7
			N–S–F_2	172.47(10)	174.5

[a] Calculated at the B3LYP/aug-cc-pVTZ level of theory.

The crystal structures of $SF_4 \cdot NC_5H_5$, $SF_4 \cdot 4\text{-}NC_5H_4(CH_3)$, and $SF_4 \cdot 4\text{-}NC_5H_4N(CH_3)_2$ contain well separated $SF_4 \cdot N$-base molecular units with a distorted square-pyramidal AX_4YE VSEPR geometries about sulfur (Figure 2), as reproduced by DFT calculations (vide infra). The VSEPR model[18] predicts that the nitrogen-base coordinates *cis* to the lone pair domain in the equatorial position, as a consequence of the weaker lone-pair domain/S---N bond pair domain repulsion compared with that between the lone-pair and the S–F domains. Upon coordination of the nitrogen-bases in the equatorial plane of SF_4, the F_1–S–F_2 angle contracts to 89.98(11) - 95.74(9)°, compared to the F_{eq}–S–F_{eq} angle in free SF_4 as determined by microwave spectroscopy (MW) (101.6(5)°)[19]/electron diffraction (ED) (103.8(6)°),[20] and X-ray diffraction (XRD) (99.6(3), 101.0(2)°).[10] In contrast, the F_3–S–F_4 moiety changes unappreciably upon adduct formation with the F_3–S–F_4 angles ranging from 169.70(14) to 172.60(10)°, as compared to 173.1(5)° in gaseous SF_4[20] and 171.6(3)/172.6(3)° in solid SF_4.[10] The axial SF_2 bonds in free SF_4 are elongated upon complexation (gaseous SF_4: 1.646(3) Å (MW)[17]/1.643(5) Å (ED),[18] solid SF_4: 1.635(4) - 1.676(5) Å (XRD),[10] S–F_3 and S–F_4 in adducts: 1.652(2) - 1.684(2) Å), with the S–F_3 and S–F_4 bond lengths being equal within ±3σ for each complex. The two symmetry-related S–F bonds of the equatorial SF_2 group in SF_4 (S–F: 1.545(3) Å (MW),[19] 1.542(5) Å (ED),[20] 1.474(6) - 1.553(4) Å (XRD)[10]) become markedly different in the adducts with one shorter bond *cis* (S–F_1: 1.526(2) to 1.561(2) Å) and one longer bond *trans* to the S---N bond (S–F_2: 1.551(2) - 1.616(2) Å) . The S---N bond lengths are equal for $SF_4 \cdot NC_5H_5$ and $SF_4 \cdot 4\text{-}NC_5H_4(CH_3)$ (2.513(3) Å) and significantly shorter than the sum of the van der Waals radii (3.35Å).[21] The adduct involving the stronger Lewis base, $SF_4 \cdot 2,6\text{-}NC_5H_4N(CH_3)_2$, presents the shortest S---N distance (2.141(2) Å), which most significantly affects the bond lengths in the SF_4 moiety, *i.e.*, the S–F_2

bond in the DMAP adduct is the longest (1.616(2) Å) in this series of adducts, consistent with donation of electron density of the strongly basic DMAP.

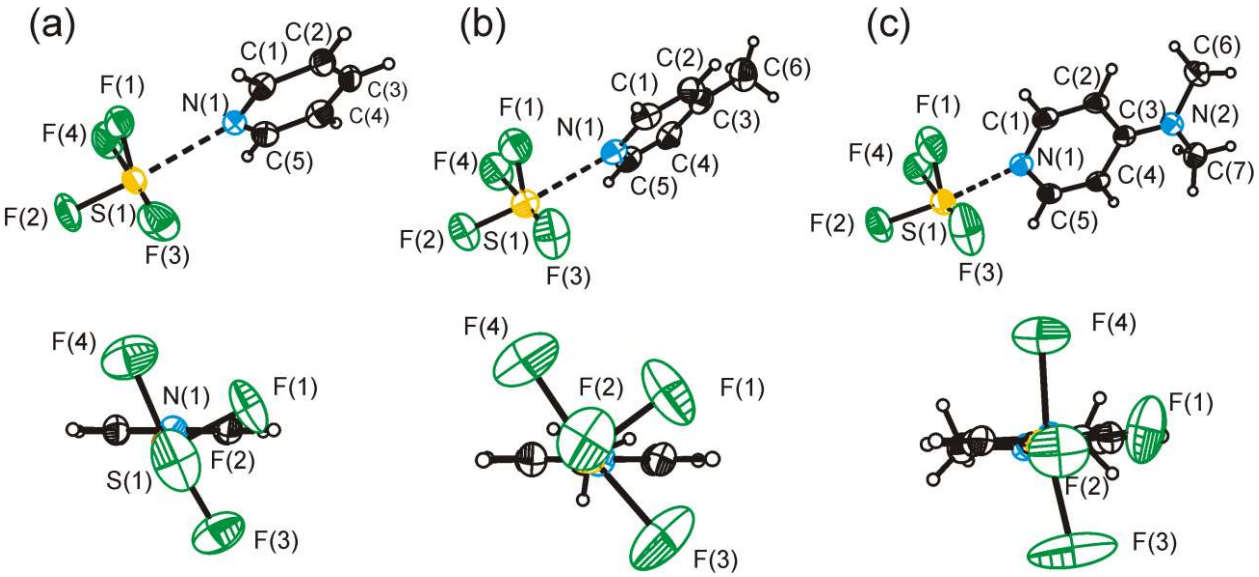

Figure 2. Thermal ellipsoid plots of (a) $SF_4 \cdot NC_5H_5$, (b) $SF_4 \cdot 4\text{-}NC_5H_4(CH_3)$, and (c) $SF_4 \cdot 4\text{-}NC_5H_4N(CH_3)_2$. Thermal ellipsoids are set at 50 % probability.

Beside the incremental changes in the bond lengths and angles in these adducts, it should be noted that the $SF_4 \cdot NC_5H_4N(CH_3)_2$ adduct adopts a unique conformation of the pyridine ring (Figure 2). The pyridine moiety is staggered in $SF_4 \cdot NC_5H_5$ and $SF_4 \cdot 4\text{-}NC_5H_4(CH_3)$, with $F_1{-}S_1{-}N_1{-}C_1$ torsion angles of 31.8(2) and 35.9(2)°, respectively, reducing the steric interactions between the pyridine ring and the *cis*-fluorine atoms. A nearly eclipsed conformation, on the other hand, is found for $SF_4 \cdot 4\text{-}NC_5H_4N(CH_3)_2$, with a $F_1{-}S_1{-}N_1{-}C_1$ torsion angle of 10.5(2)°. The conformations in the experimental solid-state structures are not reproduced by the optimized gas-phase geometries, which is in accord with the predicted shallow energy minimum for

conformational changes (see Computational Results) and, therefore, the importance of packing effects on the observed solid-state structures.

Trends in Lewis Basicity of the Nitrogen-Bases

Several approaches can be used to quantify Lewis basicity. The major impediment in the quantification of Lewis basicity/acidity is its inherent dependence on the nature of the Lewis acid/base used to form the adduct. The most extensive list for Lewis basicity is available in terms of the BF_3 affinity scale.[22] The BF_3 affinities follow the sequence with affinity values in kJ mol^{-1} given in parentheses: 4-$NC_5H_4N(CH_3)_2$ (152) > $N(C_2H_5)_3$ (136) > 4-$NC_5H_4CH_3$, (134) > NC_5H_5 (128) > 2,6-$NC_5H_3(CH_3)_2$ (98). To the best of our knowledge, no BF_3 affinity values have been determined for quinoline and isoquinoline. Although BF_3 is a harder Lewis acid than SF_4, the general sequence of donor strength can be correlated to the Raman spectroscopic and structural findings of the present and previous study.[1]

The donor strengths of the nitrogen bases have a reciprocal relationship with the S---N bond lengths (SF_4·4-$NC_5H_4N(CH_3)_2$: 2.141(2) Å, SF_4·$N(C_2H_5)_3$: 2.384(2) Å,[1] SF_4·4-$NC_5H_4(CH_3)$: 2.513(3) Å, and SF_4·NC_5H_5 2.514(2) Å). In addition, the S–F_2 bond lengths correlate well with the donor strength of the base. The magnitude of low-frequency shifts of the S–F stretching bands relative to free SF_4 can also be correlated with the donor strength of the *N*-base. For example, the S–F_1 stretching frequencies for adducts with the strongest and weakest bases appear at the lowest and highest frequencies (SF_4·4-$NC_5H_4N(CH_3)_2$: 797 cm^{-1} and SF_4·2,6-$NC_5H_3(CH_3)_2$: 861 cm^{-1}), respectively.

NMR Spectroscopy

The 4-$NC_5H_4N(CH_3)_2$, 4-$NC_5H_4CH_3$, and NC_5H_5 adducts of SF_4 were studied by ^{19}F solution NMR spectroscopy at −60 °C in excess SF_4 as the solvent. Rapid exchange was observed between adducted SF_4 and free SF_4 for solutions containing a slight excess of SF_4, as previously observed for the $SF_4 \cdot N(C_2H_5)_3$ adduct in SF_4 solvent.[1] The ^{19}F NMR spectrum of 4-methylpyridine in SF_4 (1 : 1.6 4-methylpyridine-to-SF_4 ratio) showed a broad signal for SF_4 at 56.3 ppm ($\Delta\nu_{½}$ = 4966 Hz) reflecting not only the fast exchange between fluorine environments within the SF_4 adduct, but the fast intermolecular exchange between free and adducted SF_4. In the case of pyridine, a larger excess of SF_4 was used (1 : 4.2 pyridine-to-SF_4 molar ratio), resulting in an intense broad singlet at 54.1 ppm ($\Delta\nu_{½}$ = 1128 Hz) and two low-intensity triplets corresponding to SF_4. The observation of separate resonances for the axial and equatorial fluorine environments of free SF_4 with intensities that are much smaller than expected from the excess SF_4 used can be explained by rapid intermolecular exchange between the adduct and most of the free SF_4. The two triplets, on the other hand, arise from free SF_4 that cannot diffuse fast enough through the solvent shell surrounding the adduct to partake in fast exchange.

Because of the very low solubility of $SF_4 \cdot NC_5H_4N(CH_3)_2$ in SF_4 solvent, only a very dilute sample could be prepared. The ^{19}F NMR spectrum showed two intense triplets for free SF_4 and a low-intensity broad singlet at 58.8 ppm ($\Delta\nu_{½}$ = 735 Hz). Even for the $SF_4 \cdot NC_5H_4N(CH_3)_2$ adduct, rapid exchange between the different fluorine environments in the adduct occurs at −60 °C. An intermolecular exchange mechanism cannot be excluded for this adduct.

The solution sample of $SF_4 \cdot NC_5H_5$ in SF_4 solvent was also studied by ^{1}H and ^{13}C NMR spectroscopy at −60 °C. In both NMR spectra, significant changes in chemical shifts were observed compared to neat pyridine at the same temperature. Upon adduct formation, the resonances of

ortho-, *meta*- and *para*-protons of pyridine are shifted from 8.03, 6.52, and 6.89 ppm in neat pyridine to 8.62, 7.49 and 7.87 ppm, respectively. Similar shifts were observed for the adduct between pyridine and trifluoroacetic anhydride at −78 °C, where the resonances for *ortho*-, *meta*- and *para*-protons were reported to shift from 8.03, 6.52, and 6.89 ppm in neat pyridine to 8.23, 6.93, and 7.34 ppm, respectively.[23]

The ^{13}C resonances for the *ortho*-, *meta*-, and *para*-carbons of neat pyridine (158.1, 132.0, and 145.4 ppm) are shifted to 154.6, 133.0, and 146.8 ppm for the $SF_4 \cdot NC_5H_5$ adduct. The ^{13}C NMR spectrum of the adduct between pyridine and trifluoroacetic anhydride at −78 °C exhibited similar shifts with the resonances for *ortho*-, *meta*-, and *para*-carbons being shifted from 150.0, 123.8, and 135.8 ppm in pyridine to 147.9, 123.9, and 135.9 ppm in the adduct, respectively.[23]

Computational Results.

The electronic structures of $SF_4 \cdot NC_5H_5$, $SF_4 \cdot 4\text{-}NC_5H_4(CH_3)$, $SF_4 \cdot 2,6\text{-}NC_5H_3(CH_3)_2$, and $SF_4 \cdot 4\text{-}NC_5H_4N(CH_3)_2$, as well as those of SF_4 and the respective free nitrogen-bases, were optimized in the gas phase using the B3LYP/aug-cc-pVTZ method, where each structure is a stationary point in the potential energy surface at which all frequencies are real. The optimized geometries of the $SF_4 \cdot NC_5H_5$, $SF_4 \cdot 4\text{-}NC_5H_4(CH_3)$, $SF_4 \cdot 2,6\text{-}NC_5H_3(CH_3)_2$, and $SF_4 \cdot 4\text{-}NC_5H_4N(CH_3)_2$ adducts are depicted in Figure 3 and selected calculated metric parameters are listed in Table 3. A complete list of calculated metric parameters is provided in the supporting information.

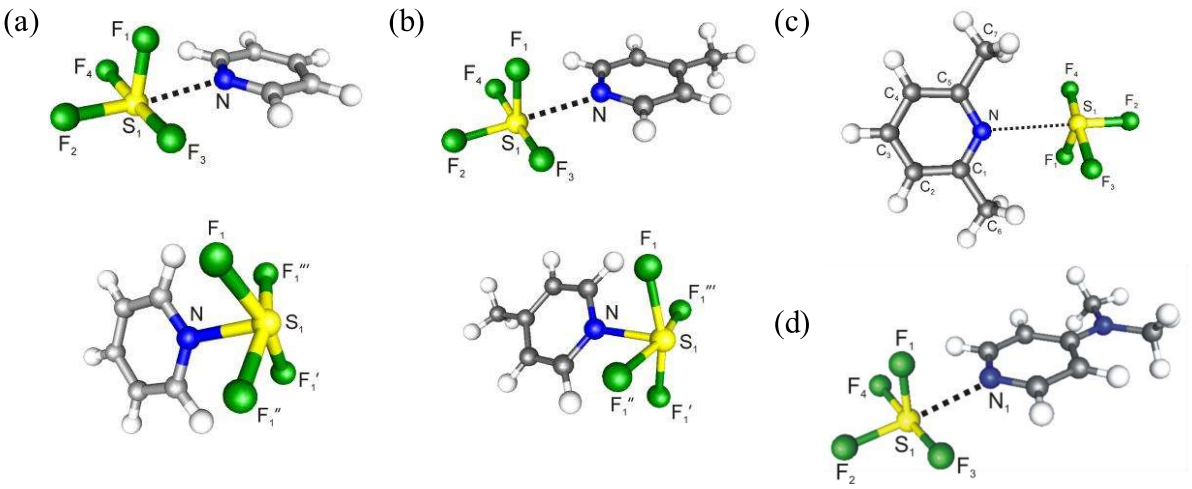

Figure 3. Optimized geometries of (a) $SF_4 \cdot NC_5H_5$ (isomer A and B), (b) $SF_4 \cdot 4\text{-}NC_5H_4(CH_3)$ (isomer A and B), (c) $SF_4 \cdot 2,6\text{-}NC_5H_3(CH_3)_2$ and (d) $SF_4 \cdot 4\text{-}NC_5H_4N(CH_3)_2$.

(a) Calculated Geometries. The geometry optimization of the SF_4·base adducts in the gas phase found two energy minima for $SF_4 \cdot NC_5H_5$ and $SF_4 \cdot 4\text{-}NC_5H_4CH_3$: a global minimum corresponding to isomer A (Scheme I) and a local minimum corresponding to isomer B (Scheme I). Isomer B was calculated to be 57.3 and 53.1 kJ/mol higher in energy than the global minima for $SF_4 \cdot NC_5H_5$ and $SF_4 \cdot 4\text{-}NC_5H_4(CH_3)$, respectively. For the $SF_4 \cdot 2,6\text{-}NC_5H_3(CH_3)_2$, and $SF_4 \cdot 4\text{-}NC_5H_4N(CH_3)_2$ adducts, only one minimum-energy geometry (isomer A) was obtained, irrespective of the starting geometry used in the optimization. The optimized geometries (isomer A) for $SF_4 \cdot NC_5H_5$, $SF_4 \cdot 4\text{-}NC_5H_4(CH_3)$ and $SF_4 \cdot 4\text{-}NC_5H_4N(CH_3)_2$ are in good agreement with those obtained by X-ray crystallography (vide supra), even though all the bond lengths are somewhat overestimated. The largest difference between calculated and observed geometries occurs with the $SF_4 \cdot 4\text{-}NC_5H_4N(CH_3)_2$ adduct, for which, coincidentally, the Lewis acid-base interaction was significantly underestimated by the calculations. In this case, the predicted S---N distance (2.453 Å) is significantly longer than the experimental distance (2.141(2) Å). Consequently, the S–F_2 bond, *i.e.*, the S–F bond *trans* to

the S---N interaction, is predicted to be shorter than the experimental value. The overestimation of the S---N bond length was previously reported for the $SF_4 \cdot N(C_2H_5)_3$ adduct.[1]

The conformation of the pyridine moieties in the pyridine, 4-methylpyridine, and DMAP adducts with respect to SF_4 was predicted to be eclipsed with F1−S1−N1−C1 torsion angles of 92.5, 91.6, and 91.9°, respectively. In the $SF_4 \cdot$2,6-$NC_5H_3(CH_3)_2$ adduct, however, the two *ortho*-methyl groups in 2,6-dimethylpyridine were predicted to be staggered with respect to the equatorial fluorines of SF_4 with a F1−S1−N1−C1 torsion angle of 45.9°. The optimized gas-phase conformations for the $SF_4 \cdot NC_5H_5$, $SF_4 \cdot$4-$NC_5H_4(CH_3)$ and $SF_4 \cdot$4-$NC_5H_4N(CH_3)_2$ adducts stand in stark contrast with respect to those obtained by X-ray crystallography, which show staggered conformations. The energy barrier of rotation about the S−N bond for $SF_4 \cdot NC_5H_5$ was predicted to be 5.2 kJ mol^{-1}. The conformation of the optimized geometries for $SF_4 \cdot NC_5H_5$, $SF_4 \cdot$4-$NC_5H_4(CH_3)$, and $SF_4 \cdot$4-$NC_5H_4N(CH_3)_2$ in the gas phase can be readily understood to result from an interaction of the HOMO of the SF_4 group with the LUMO of the pyridine moiety (Scheme II). Furthermore, this conformation is stabilized by two very weak C−H···F−S interactions, inferred from the quantum theory of atoms-in-molecules (QTAIM) analysis (vide infra). Hence, the crystal structures must be explained in terms of packing effects. A recent computational study (MP2/aug-cc.pVDZ) of Lewis acid-base adducts between SF_4 and amines, as well as cyclic nitrogen bases included the $SF_4 \cdot NC_5H_5$ adduct.[24] The same conformer was found as in the present study. The predicted S---N bond length using the MP2 method (2.308 Å), however, greatly underestimated the experimental distance (2.514 Å).

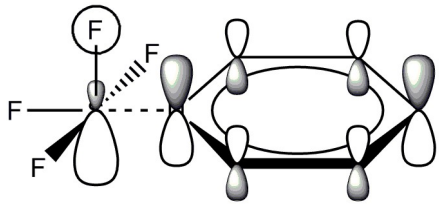

Scheme II

Attempts at optimizing the gas-phase geometries for SF_4 adducts with quinoline or isoquinoline were unsuccessful. In both cases, the SF_4 and the nitrogen-base dissociated during the optimization process, which is consistent with failure to observe these adducts by low-temperature Raman spectroscopy.

In contrast to the global minimum-energy geometry, the local minimum (isomer B) exhibits strong S–N bonding interactions (calculated bond lengths: 1.971 Å for $SF_4 \cdot NC_5H_5$ and 1.931 Å for $SF_4 \cdot 4\text{-}NC_5H_4(CH_3)$), which are *trans* to the lone pair. The predicted S−F bond lengths in this isomer of $SF_4 \cdot NC_5H_5$ and $SF_4 \cdot 4\text{-}NC_5H_4(CH_3)$ are elongated (1.724 and 1.736 Å, respectively) with respect to those of free SF_4, and the square SF_4 moiety is slightly pyramidalized with the S−F bond domains experiencing a larger repulsion from the lone pair (N−S−F angles: 82.0 and 82.8°, respectively).

(b) Vibrational Frequencies. The predicted vibrational frequencies and Raman and infrared intensities are given in Table 1 and supporting information Tables S1 - S4, together with an approximate mode description.

The calculations in this study generally underestimate experimental S−F stretching frequencies with the exception of the $SF_4 \cdot 4\text{-}NC_5H_4N(CH_3)_2$ adduct. This results from the significant underestimation of the Lewis acid-base interaction in these adducts by the DFT calculations (vide supra).

Vibrational frequencies of the isomer B of $SF_4 \cdot NC_5H_5$ and $SF_4 \cdot 4\text{-}NC_5H_4(CH_3)$ have also been calculated. The S–N stretching frequencies for this isomer of $SF_4 \cdot NC_5H_5$ and $SF_4 \cdot 4\text{-}NC_5H_4(CH_3)$ are predicted at 190 and 206 cm^{-1}, respectively, which are much higher than those for isomer A (70 and 68 cm^{-1}, respectively), reflecting the stronger predicted S–N bonding interactions for isomer B. The calculations predict that two SF_4 stretching modes should be observable by Raman spectroscopy for each adduct ($SF_4 \cdot NC_5H_5$: 678 and 455 cm^{-1} and $SF_4 \cdot 4\text{-}NC_5H_4(CH_3)$: 650 and 440 cm^{-1}, corresponding to the symmetric and asymmetric SF_4 stretching modes, respectively). A pair of nearly degenerate SF_4 stretching modes were predicted to have negligible Raman intensities, but large infrared intensities. Since the Lewis acid-base interactions are calculated to be much stronger in isomer B than in isomer A, the predicted frequency of the NC_5 ring breathing mode is significantly higher for isomer B ($SF_4 \cdot NC_5H_5$: 1042 cm^{-1} and $SF_4 \cdot 4\text{-}NC_5H_4(CH_3)$: 1050 cm^{-1}), being 16 and 22 cm^{-1} higher than the predicted frequencies for isomer A. Since none of these predicted Raman bands for isomer B were observed in the spectra of $SF_4 \cdot NC_5H_5$ and $SF_4 \cdot 4\text{-}NC_5H_4(CH_3)$, the experimental results clearly indicate the exclusive presence of isomer A.

(c) Bond Energies, Bond Dissociation Enthalpies and Gibbs Free Energies. The predicted bond energies, bond dissociation enthalpies and Gibbs free energies of the S---N bonds are listed in Table S11 for the $SF_4 \cdot NC_5H_5$, $SF_4 \cdot 4\text{-}NC_5H_4(CH_3)$, $SF_4 \cdot 2,6\text{-}NC_5H_3(CH_3)_2$, and $SF_4 \cdot 4\text{-}NC_5H_4N(CH_3)_2$ adducts.

The predicted bond dissociation enthalpies for the adducts adopting the experimental geometries, *i.e.*, isomer A, range from 12.03 to 30.99 kJ mol^{-1}. In contrast, the calculated S–N bond dissociation enthalpies for isomer B of $SF_4 \cdot NC_5H_5$ and $SF_4 \cdot 4\text{-}NC_5H_4(CH_3)$ are significantly exothermic, reflecting the thermodynamic instability of the isomer B. It is noteworthy that the calculated $\Delta_{BD}H°$ values for $SF_4 \cdot 4\text{-}NC_5H_4N(CH_3)_2$, as found in the case of $SF_4 \cdot N(C_2H_5)_3$,[1] are

significantly underestimating the expected experimental values, since the S---N distance for these two adducts have been predicted to be too long by the DFT calculations. The strength of the Lewis acid-base interaction is comparable to that of hydrogen bonds. For example, the calculated dissociation energy for the HO–H···OH_2 (20 kJ mol^{-1})[25] is very similar to those of the $SF_4 \cdot NC_5H_5$ and $SF_4 \cdot 4$-$NC_5H_4(CH_3)$ adducts. The lower bond dissociation enthalpy of the 2,6-dimethylpyridine adduct (12.03 kJ mol^{-1}) is likely a consequence of the steric effects of the two methyl substituents in the 2,6-positions.

(d) Atoms in Molecules Analysis. The wavefunctions of SF_4, the adducts, as well as the free nitrogen-bases were analyzed by Bader's quantum theory of atoms in molecules (QTAIM).[26] For comparison purposes, $N(C_2H_5)_3$ and $SF_4 \cdot N(C_2H_5)_3$, whose characterization has previously been reported,[1] were also analyzed by QTAIM. Molecular graphs of SF_4, NC_5H_5, and $SF_4 \cdot NC_5H_5$ are given in Figure 4, along with the atomic basin charges, the charges at the bond critical points and the bond ellipticities. The full list of atomic basin charges, electron densities at the bond critical points ($\rho(r)$) and bond ellipticities (λ) are given in Tables S8 - S12 and the molecular graphs are depicted in Figures S5 – S8.

Sulfur tetrafluoride has previously been analyzed using QTAIM by Gillespie *et al.* at the HF/6-311F** level of theory.[27] The AIM results in this study are in good agreement with those reported previously, where any deviations result from the difference in the level of theory used. The formation of the adducts is accompanied by a reduction in the atomic basin charges on sulfur (SF_4: 2.648, $SF_4 \cdot NC_5H_5$: 2.548, $SF_4 \cdot 4$-$NC_5H_4(CH_3)$: 2.548, $SF_4 \cdot 2,6$-$NC_5H_3(CH_3)_2$: 2.600, $SF_4 \cdot 4$-$NC_5H_4N(CH_3)_2$: 2.506, $SF_4 \cdot N(C_2H_5)_3$: 2.499), as the nitrogen serves as an attractor. Correspondingly, there is an increase in negative charge in the nitrogen atomic basin upon adduct formation. The atomic basin charge on F_1 becomes more negative upon adduct formation (SF_4:

−0.670, $SF_4 \cdot NC_5H_5$: −0.681, $SF_4 \cdot 4\text{-}NC_5H_4(CH_3)$: −0.681, $SF_4 \cdot 2,6\text{-}NC_5H_3(CH_3)_2$: −0.681, $SF_4 \cdot 4\text{-}NC_5H_4N(CH_3)_2$: −0.683, $SF_4 \cdot N(C_2H_5)_3$: −0.685), whereas those of F_2, F_3, and F_4 are unaltered. Interestingly, the atomic basin charges on F_1 does not change significantly between the adducts, indicating that any perturbation in the F_1 atomic basin properties are largely the results of structural changes, thereby rendering the influence of donor strength as negligible. The total charge on the SF_4 and the base moieties, as the sum of the respective atomic basin charges, describe the degree of charge donation from the base towards the SF_4 moiety. The charge increase in the SF_4 moiety when adducted to stronger bases reflects the increased charge donation by the stronger bases: −0.066 ($SF_4 \cdot 2,6\text{-}NC_5H_3(CH_3)_2$); −0.115 ($SF_4 \cdot NC_5H_5$); −0.124 ($SF_4 \cdot 4\text{-}NC_5H_4(CH_3)$); −0.157 ($SF_4 \cdot 4\text{-}NC_5H_4N(CH_3)_2$); and −0.168 ($SF_4 \cdot N(C_2H_5)_3$).

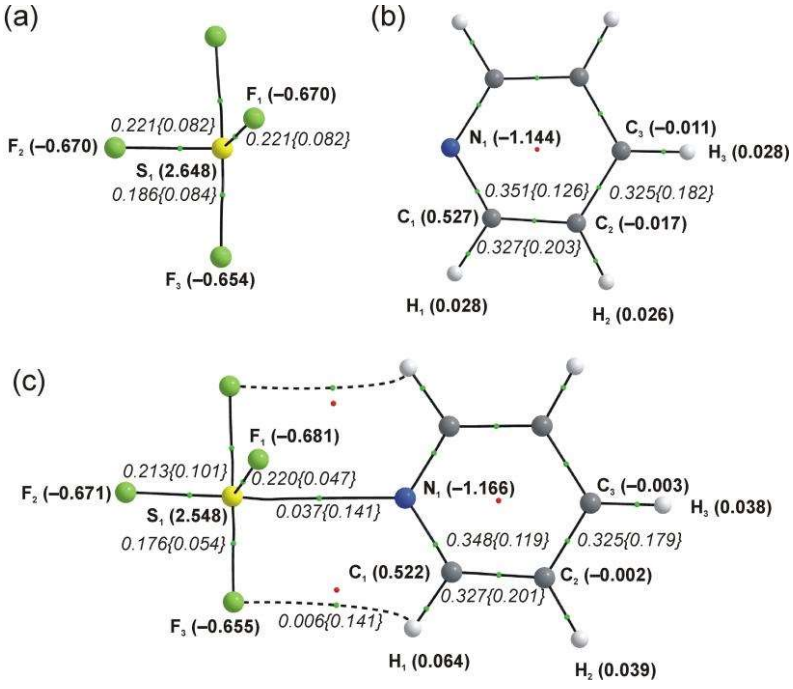

Figure 4. Molecular graphs for (a) SF_4, (b) NC_5H_5, and (c) $SF_4 \cdot NC_5H_5$, showing the bond paths, the bond critical points (green spheres) and ring critical points (red spheres). The atomic

basin charges are indicated in parentheses adjacent to the atom labels, and the electron densities ($\rho(r)$) at the bond critical points are given in italics along with their corresponding ellipticities (λ) in brackets. The values for the symmetry related atoms and bond critical points are omitted.

In QTAIM, the charge density ($\rho(r)$) at the bond critical point is correlated to the strength of a bond. For SF_4, larger $\rho(r)$ values are found for the shorter equatorial S−F bonds ($S-F_{eq}$: 0.221 a.u.; $S-F_{ax}$: 0.186 a.u.). In each adduct, the $S-F_1$ bond has the largest $\rho(r)$ value compared to the other S−F bonds, in agreement with the $S-F_1$ bond being shorter than the other S−F bonds. The electron density at the $S-F_1$ bond critical point decreases slightly for adducts with stronger bases (SF_4·2,6-$NC_5H_3(CH_3)_2$: 0.221 a.u., SF_4·NC_5H_5: 0.220 a.u.; SF_4·4-$NC_5H_4(CH_3)$: 0.220 a.u., SF_4·4-$NC_5H_4N(CH_3)_2$: 0.218 a.u., SF_4·$N(C_2H_5)_3$: 0.217 a.u.), paralleling the trend in increasing predicted $S-F_1$ bond lengths. The $\rho(r)$ values at the $S-N_1$ bond critical points are small (SF_4·NC_5H_5 – isomer A: 0.037 a.u.; SF_4·4-$NC_5H_4N(CH_3)_2$: 0.048 a.u., SF_4·$N(C_2H_5)_3$: 0.036 a.u.), reflecting weakness in the interaction between sulfur and nitrogen. For isomer B of SF_4·NC_5H_5 and SF_4·4-$NC_5H_4(CH_3)$, the electron densities at the $S-N_1$ bond critical points are close to those at the S−F bond critical points, consistent with the S−N bond length predicted to be shorter in this isomer. The ellipticity of $\rho(r)$ provides information about the π-character of a bond. The ellipticities at the $S-N_1$ and $S-F_1$ bond critical points in the adducts (isomer A) are substantially larger than those of the $S-F_2$, $S-F_3$, and $S-F_4$ bonds. The larger ellipticity implies appreciable π-contribution in $S-N_1$ and $S-F_1$ bonding, which is in agreement with Scheme II. For the adducts, some hydrogen atoms on the base are close enough to F_3 and F_4 to give rise to F···H bond critical points and ring critical points (Figure 4 and S8). In SF_4·2,6-$NC_5H_3(CH_3)_2$ and SF_4·$N(C_2H_5)_3$, hydrogen atoms are close enough to F_1 to form additional F···H bond critical points, resulting in ring critical points and cage critical points (Figure

S6 and S7). The electron densities at these F···H bond critical points are extremely small ($SF_4 \cdot NC_5H_5$: 0.006 a.u.) and, therefore, represent very weak interactions. These extremely weak hydrogen-bonding interactions can be a significant factor in stabilizing the predicted gas-phase conformation, but are likely too weak to play a similar role in the condensed phase.

In QTAIM, the minima and maxima in the Laplacian of the electron density ($\nabla^2\rho$) represent regions of charge concentration and depletion, respectively.[28] Figure 5 shows the contour maps of the $\nabla^2\rho$ for SF_4, $SF_4 \cdot NC_5H_5$, and $SF_4 \cdot 4\text{-}NC_5H_4N(CH_3)_2$ in the F_1SF_2 plane. Near sulfur, four bonded and one non-bonded valence shell charge concentration (VSCC) are seen in SF_4 and the adducts (only two bonded VSCC are shown in Figure 4). The non-bonded VSCC can be associated with the lone pair on sulfur. When forming the S---N dative bond, the non-bonded VSCC on sulfur is slightly distorted, indicating that the adducted nitrogen base has a small effect on the lone pair domain. Even for the strongest base (DMAP) considered, the VSCC does not shift dramatically *trans* to the $S{-}F_1$ bond, as would be eluded via a simple description of a distorted square pyramidal AX_4YE VSEPR geometry.

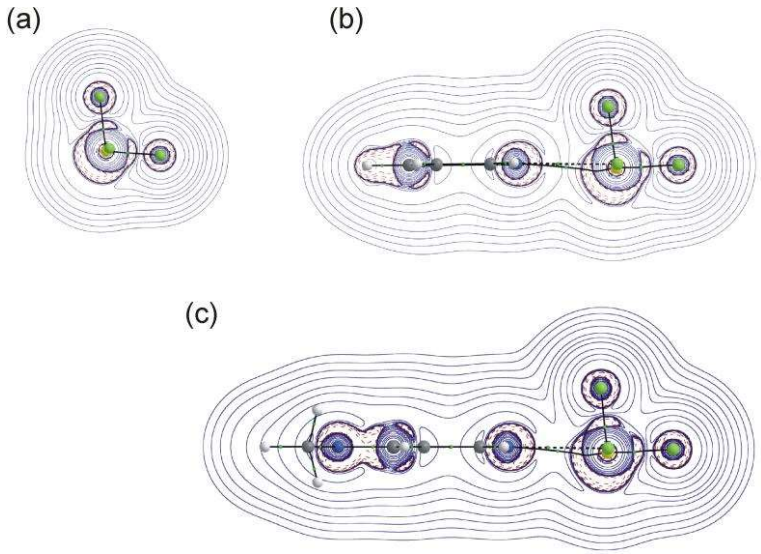

Figure 5. Contour map of $\nabla^2\rho$ for (a) SF_4, (b) $SF_4{\cdot}NC_5H_5$, and (c) $SF_4{\cdot}4\text{-}NC_5H_4N(CH_3)_2$ within the F_1SF_2 plane. The pyridine and DMAP molecules are perpendicular to the plane. Solid contour lines denote positive values of $\nabla^2\rho$, whereas dashed contour lines denote negative values of $\nabla^2\rho$, *i.e.*, areas of charge concentration. Bond paths are drawn as solid lines except for the H···F bond paths, which are shown as dashed lines.

Conclusion. Adducts of SF_4 with pyridine, 2,6-dimethylpyridine, 4-methylpyridine, and 4-dimethylaminopyridine were isolated at low temperature and unambiguously characterized by Raman spectroscopy. The crystal structures of $SF_4{\cdot}NC_5H_5$, $SF_4{\cdot}NC_5H_4(CH_3)$, and $SF_4{\cdot}NC_5H_4N(CH_3)_2$ provide conclusive structural information for these adducts. This work represents the first proof for the Lewis acid-base interaction between SF_4 and pyridine and pyridine-derivatives. Insights gained into the interactions between SF_4 and organic Lewis bases are important milestones in elucidating reaction pathways in organic reactions involving SF_4, such as deoxofluorination reactions. The weak dative S←N bonding interactions in these adducts observed in this work is only the second such conclusive finding, which follows our communication regarding the triethylamine adduct of SF_4, of such bonding modalities, which are new in the rich chemistry of F−S−N compounds. Analysis of the computed wavefunction by the QTAIM, showed that the adducted nitrogen bases impose minimal distortion on the non-bonded valence shell charge concentration on sulfur, which for all intents and purposes can be regarded as representing the lone pair. In addition, several metric and spectroscopic parameters were identified to ascertain the Lewis basicity of nitrogen bases towards Lewis acidic SF_4, which will prove helpful in the future study of Lewis acid base adducts of SF_4.

Experimental

Materials and Apparatus. All volatile materials were handled (a) on a Pyrex vacuum line equipped with glass/Teflon J. Young valves and (b) a vacuum line constructed of nickel, stainless steel, and FEP. Non-volatile materials were handled in the dry nitrogen atmosphere of a drybox (Omni Lab, Vacuum Atmospheres). Reaction vessels and NMR sample tubes were fabricated from ¼-in. o.d. and 4-mm o.d. FEP tubing, respectively, and outfitted with Kel-F valves. All reaction vessels and sample tubes were rigorously dried under dynamic vacuum prior to passivation with 1 atm F_2 gas.

The nitrogen bases were purchased from Sigma-Aldrich. 4-Dimethylaminopyridine was dried under vacuum, while 2,6-dimethylpyridine was used as received. 4-Methylpyridine was purified by vacuum distillation onto freshly cut potassium, followed by distillation onto dry 4Å-molecular sieves. Pyridine was dried over 4Å molecular sieves, followed by distillation onto calcium hydride. Quinoline and isoquinoline were used as received. Sulfur tetrafluoride (Ozark-Mahoning Co.) was purified by passing the gas through an FEP U-trap containing activated charcoal. Traces of thionyl fluoride and sulfur hexafluoride were present in the sulfur tetrafluoride, as observed by ^{19}F NMR spectroscopy, but did not interfere with the chemistry.

$SF_4 \cdot NC_5H_5$: In a typical experiment, pyridine (0.014g, 0.18 mmol) was vacuum distilled into a ¼-in. FEP reactor equipped with a Kel-F valve. A large excess of SF_4 was vacuum-distilled onto the frozen pyridine at –196 °C. Upon melting of SF_4 at –120 °C, pyridine reacted with SF_4 forming a clear colorless solution. The sample was warmed to –90 °C to ensure complete reaction, and excess SF_4 was removed under dynamic vacuum, yielding 0.038 g of a white solid, corresponding to a NC_5H_5 to SF_4 molar ratio of 1 to 1.2. It proved to be difficult to isolate the pure $SF_4 \cdot NC_5H_5$

adduct, since SF_4 could slowly be removed from the adduct while pumping on the solid adduct at –80 °C, reflecting the weakness of the Lewis acid-base interaction. Fluorine-19 NMR spectroscopy at –60 °C in SF_4 (1 : 4.2 pyridine-to-SF_4 molar ratio): singlet at 54.1 ppm ($\Delta\nu_{1/2}$ = 1128 Hz).

$SF_4 \cdot NC_5H_4(CH_3)$: In a typical experiment, 4-methylpyridine (0.094 g, 1.0 mmol) was vacuum distilled into a ¼-in. FEP reactor equipped with a Kel-F valve. A three molar excess of SF_4 was vacuum-distilled onto the frozen 4-methylpyridine at –196 °C. Warming the reaction mixture to –60 °C resulted in the slow dissolution of solid 4-methylpyridine in liquid SF_4, yielding a clear colorless solution. The sample was cooled to –80 °C inducing the formation of large needle-like crystals. Excess SF_4 was removed under dynamic vacuum at –80 °C, yielding, essentially quantitatively, 0.20 g of a white solid $SF_4 \cdot NC_5H_4(CH_3)$ ($NC_5H_4(CH_3)$ to SF_4 molar ratio of 1 to 1.0). Fluorine-19 NMR spectroscopy at –60 °C in SF_4 (1 : 1.6 4-methylpyridine -to-SF_4 ratio): singlet at 56.3 ppm ($\Delta\nu_{1/2}$ = 4966 Hz).

$SF_4 \cdot 2,6\text{-}NC_5H_3(CH_3)_2$: In a typical experiment, anhydrous 2,6-dimethylpyridine (0.047 g, 0.44 mmol) was syringed into a ¼-in. FEP reactor equipped with a Kel-F valve inside a glove bag containing dry nitrogen. A five molar excess of SF_4 was vacuum-distilled onto the frozen 2,6-dimethylpyridine at –196 °C. Warming the reactor to –80 °C while agitating caused the white solid 2,6-dimethylpyridine to slowly dissolve in the liquid SF_4 forming a clear colorless solution. The sample was cooled to –90 °C and placed under dynamic vacuum, yielding 0.10 g of a white solid, corresponding to a 2,6-$NC_5H_3(CH_3)_2$ to SF_4·molar ratio of 1 to 1.1. Fluorine-19 NMR spectroscopy at –60 °C in SF_4 (1 : 1.3 2,6-dimethylpyridine -to-SF_4 ratio): singlet at 55.7 ppm ($\Delta\nu_{1/2}$ = 929 Hz).

$SF_4 \cdot 4\text{-}NC_5H_4N(CH_3)_2$: In a typical experiment, 4-dimethylaminopyridine (0.065 g, 0.53 mmol) was added inside a dry box into a ¼-in. FEP reactor equipped with a Kel-F valve. A large

excess of SF_4 was vacuum-distilled onto the frozen 4-dimethylaminopyridine at −196 °C. Upon melting of SF_4 at −120 °C, the crystalline 4-dimethylaminopyridine slowly reacted with SF_4 forming a fine white suspension, which eventually formed a layer on top of clear colorless liquid SF_4. The sample was warmed to −60 °C and mixed, followed by removal of excess SF_4 under dynamic vacuum at −80 °C, yielding 0.13 g of a white solid, corresponding to a 4-$NC_5H_4N(CH_3)_2$ to SF_4·molar ratio of 1 to 1.1. Fluorine-19 NMR spectroscopy at −60 °C in a very large excess of SF_4: SF_4·$NC_5H_4N(CH_3)_2$, singlet at 58.8 ppm ($\Delta\nu_{½}$ = 735 Hz), SF_4, triplets at 84.3 and 31.8 ppm, $^2J(^{19}F\text{-}^{19}F)$ = 75 Hz.

Reactions with quinoline and isoquinoline: In two separate reactions, quinoline (0.033g, 0.25 mmol) and isoquinoline (0.077 g, 0.60 mmol) were combined with approximately 0.26 mmol and 0.95 mmol of SF_4, respectively, in ¼-in. FEP reactors equipped with a Kel-F valve. The reaction mixtures were allowed to warm to −70 °C, resulting in pale brown solutions. Raman spectra of the reactions mixtures at −100 °C only showed bands of the reactants.

NMR spectroscopy: All NMR spectra were recorded unlocked on a 300 MHz Bruker Avance II NMR spectrometer equipped with a 5-mm broad band probe. Fluorine-19 NMR spectra were referenced externally to neat $CFCl_3$ at room temperature. Proton and ^{13}C NMR spectra were referenced externally to neat TMS. In the ^{19}F NMR spectra in SF_4 solvent at −78 °C, trace amounts of SOF_2 (70.9 ppm) and SF_6 (55.8 ppm) were observed, which are contaminants in commercial SF_4 and which do not interfere with the reported chemistry.

Raman spectroscopy: All Raman spectra were recorded on a Bruker RFS 100 FT Raman spectrometer with a quartz beam splitter, a liquid-nitrogen cooled Ge detector, and R-496 temperature accessory. The actual usable Stokes range was 50 to 3500 cm^{-1}. The 1064-nm line of

an Nd:YAG laser was used for excitation of the sample. The Raman spectra were recorded at –100 °C with a spectral resolution of 2 cm^{-1} using laser powers of 150 mW.

X-ray Crystallography: Crystals of $SF_4 \cdot NC_5H_5$ and $SF_4 \cdot 4\text{-}NC_5H_4(CH_3)$ were grown by slow evaporation of excess SF_4 at –118 °C in a ¼-in. o.d. FEP reactor and allowed to warm to –90 °C. Crystals of $SF_4 \cdot 4\text{-}NC_5H_4N(CH_3)_2$ were grown from CH_2Cl_2 from −60 to −80 °C. Crystals were mounted at low temperature under a stream of dry cold nitrogen as previously described.[29] The crystals were centered on a Bruker SMART APEX II diffractometer, controlled by the APEX2 Graphical User Interface software.[30] The program SADABS[31] was used for the scaling of diffraction data, the application of a decay correction, and a multi-scan absorption correction. The program SHELXS-97 (Sheldrick, 2008)[32] was used for both solution and refinement. Structure solutions were obtained by direct methods. CCDC 1037495, 1037496, and 1037497 contain the crystallographic data for $SF_4 \cdot NC_5H_5$, $SF_4 \cdot 4\text{-}NC_5H_4(CH_3)$, and $SF_4 \cdot 4\text{-}NC_5H_4N(CH_3)_2$. These data can be obtained free of charge from The Cambridge Crystallographic Data Centre via www.ccdc.cam.ac.uk/data_request/cif.

Computational Methods. All optimized geometries and frequencies were calculated at the density functional theory (DFT) level by use of the B3LYP method. The standard all-electron aug-cc-pVTZ basis sets, as implemented in the Gaussian program, were used for sulfur, fluorine, nitrogen, carbon and hydrogen were used.[33] Quantum-chemical calculations were carried out using the programs Gaussian 09.[33] The geometries were fully optimized using analytical gradient methods. The vibrational frequencies were calculated at the B3LYP level using the appropriate minimized structure, and the vibrational mode descriptions were assigned with the aid of Gaussview.[34] The geometries of two isomers, one with a nearly square planar SF_4 geometry and one with retention of the SF_4 seesaw geometry, were investigated. For $SF_4 \cdot 2,6\text{-}NC_5H_3(CH_3)_2$, and

$SF_4 \cdot 4\text{-}NC_5H_4N(CH_3)_2$, both starting geometries converged to the same square pyramidal geometry also observed experimentally. For the $SF_4 \cdot NC_5H_5$, $SF_4 \cdot 4\text{-}NC_5H_4CH_3$ adducts, two minima were obtained. The conformational energy barrier for the pyridine moiety in the $SF_4 \cdot NC_5H_5$ adduct was calculated by rotating about the S–N bond in 10° steps starting with the experimental F1–S1–N1–C1 torsion angle. The wavefunctions obtained from the DFT calculations were analysed according to the quantum theory of atoms in molecules (QTAIM)[26] using the AIM11/AIMStudio suite of programs.[35]

Acknowledgements

We thank the Natural Sciences and Engineering Research Council of Canada (M.G. and P. H.). The computations were conducted with the aid of the facilities of the Shared Hierarchical Academic Research Computing Network (SHARCNET: www.Sharcnet.ca). The authors thank Prof. Stacey Wetmore for giving S.S.H. time to help with the QTAIM analysis in this study.

References:

[1] J. T. Goettel, P. Chaudhary, P. Hazendonk, H. P. A. Mercier, M. Gerken, *Chem. Commun.* **2012,** *48*, 9210-9122.

[2] (a) E. L. Muetterties, *J. Am. Chem. Soc.* **1960**, *82*, 1082-1087; (b) E. L. Muetterties, C. Ford, W. D. Philips, W. C. Smith US Patent 2,897,055, **1959**.

[3] D. K. Padma, *J. Fluorine Chem.* **1974**, *4*, 441-443.

[4] C. S. Sass, B. S. Ault, *J. Phys. Chem.* **1985**, *89*, 1002-1006.

[5] R. Tunder, B. Siegel, *J. Inorg. Nucl. Chem.* **1963**, *25*, 1097-1098.

[6] C. W. Tullock, D. D. Coffman, E. L. Muetterties, *J. Am. Chem. Soc.* **1964**, *86*, 357-361.

[7] J. Bittner, J. Fuchs, K. Seppelt, *Z. Anorg. Allg. Chem.* **1988**, *557*, 182-190.

[8] W. Heilemann, R. Mews, S. Pohl, W. Saak, *Chem. Ber.* **1989**, *122*, 427-432.

[9] M. Clark, C. J. Kellen-Yuen, K. D. Robinson, H. Zhang, Z.-Y. Yang, K. V. Madappat, J. W. Fuller, J. L. Atwood, J. S. Thrasher, *Eur. J. Solid State Inorg. Chem.* **1992**, *29*, 809-833.

[10] J. T. Goettel, N. Kostiuk, M. Gerken, *Angew. Chem. Int. Ed.* **2013**, *52*, 8037-8040.

[11] W. C. Smith, *Angew. Chem. Int. Ed. Engl.* **1962**, *1*, 467-475.

[12] B. Cohen, A. G. MacDiarmid, *J. Chem. Soc. (A)* **1966**, 1780-1784.

[13] V. N. Filimonov, D. S. Bystrov, *Opt. Spectrosc.***1962**, 12, 31-35.

[14] J. Nieboer, X. Yu, P. Chaudhary, H. P. A. Mercier, M. Gerken, *Z. Anorg. Allg. Chem.* **2012**, *638*, 520-525.

[15] M. Taillandier, E. Taillandier, *Spectrochim. Acta A* **1969**, *25A*, 1807-1814.

[16] (a) K. O. Christe, E. C. Curtis, C. J. Schack, S. J. Cyvin, J. Brunvoll, W. Sawodny, *Spectrochim. Acta* **1976**, *32A*, 1141-1147; (b) K .O. Christe, H. WIllner, W. Sawodny, *Spectrochim. Acta* **1979**, *35A*, 1347-1351.

[17] K. O. Christe, Z. Zhang, J. A. Sheehy, R. Bau, *J. Am. Chem. Soc.* **2001**, *123*, 6338-6348.

[18] R. J. Gillespie, I. Hargittai, *The VSEPR Model of Molecular Geometry*, Allyn and Bacon,, Needham Heights, **1991**.

[19] W. M. Tolles, W. D. Gwinn, *J. Chem. Phys.* **1962**, *36*, 1119-1121.

[20] K. Kimura, S. H. Bauer, *J. Chem. Phys.* **1963**, *39*, 3172-3178.

[21] A. Bondi, *J. Phys. Chem.*, **1964**, *68*, 441-451.

[22] *Lewis Basicity and Affinity Scales* (Eds.: C. Laurence, J.-F. Gal), Wiley, Chichester, **2010**, chapt 3.

[23] U. Anthoni, D. Christensen, C. Christophersen, P. H. Nielsen, *Acta Chem. Scand.* **1995**, *49*, 203.

[24] V. d. P. N. Nizko, S. Scheiner, *J. Phys. Chem. A* **2014**, *118*, 10849-10856.

[25] M. Sodupe, A. Oliva, J. Bertran, *J. Am. Chem. Soc.* **1994**, *116*, 8249-8258.

[26] R. F. W. Bader, *Atoms in Molecules: A Quantum Theory*, Oxford University Press, Oxford, **1990**.

[27] R. J. Gillespie, I. Bytheway, R. S. DeWitte, R. F. W. Bader, *Inorg. Chem.* **1994**, *33*, 2115-2121.

[28] R. F. W. Bader, R. J. Gillespie, P. J. MacDougall, *J. Am. Chem. Soc.* **1988**, *110*, 7329-7336.

[29] M. Gerken, D. A. Dixon, G. J. Schrobilgen, *Inorg. Chem.* **2000**, *39*, 4244-4255.

[30] *APEX* 2, Version 2.2-0; Bruker AXS Inc.: Madison, WI, **2007**.

[31] G. M. Sheldrick, *SADABS*, Version 2007/4, Bruker ACS Inc.; Madison, WI, **2007**.

[32] G. M. Sheldrick, *SHELXTL97*, University of Göttingen, Germany, **2007**.

[33] Gaussian 09, Revision C.01, M. J. Frisch, G. W. Trucks, H. B. Schlegel, G. E. Scuseria, M. A. Robb, J. R. Cheeseman, G. Scalmani, V. Barone, B. Mennucci, G. A. Petersson, H. Nakatsuji, M. Caricato, X. Li, H. P. Hratchian, A. F. Izmaylov, J. Bloino, G. Zheng, J. L. Sonnenberg, M. Hada, M. Ehara, K. Toyota, R. Fukuda, J. Hasegawa, M. Ishida, T. Nakajima, Y. Honda, O. Kitao, H. Nakai, T. Vreven, J. A. Montgomery, Jr., J. E. Peralta, F. Ogliaro, M. Bearpark, J. J. Heyd, E. Brothers, K. N. Kudin, V. N. Staroverov, T. Keith, R. Kobayashi, J. Normand, K. Raghavachari, A. Rendell, J. C. Burant, S. S. Iyengar, J. Tomasi, M. Cossi, N. Rega, J. M. Millam, M. Klene, J. E. Knox, J. B. Cross, V. Bakken, C. Adamo, J. Jaramillo, R. Gomperts, R. E. Stratmann, O. Yazyev, A. J. Austin, R. Cammi,

C. Pomelli, J. W. Ochterski, R. L. Martin, K. Morokuma, V. G. Zakrzewski, G. A. Voth, P. Salvador, J. J. Dannenberg, S. Dapprich, A. D. Daniels, O. Farkas, J. B. Foresman, J. V. Ortiz, J. Cioslowski, and D. J. Fox, Gaussian, Inc., Wallingford CT, 2010.

[34] *GaussView*, release 3.0; Gaussian Inc.; Pittsburgh, PA, 2003.

[35] AIM11 (Version 14.06.21), Todd A. Keith, TK Gristmill Software, Overland Park KS, USA **2014** (aim.tkgristmill.com).